Identification and analysis of static and dynamic magnetization behavior sensitive to surface laser treatments within the electromagnetic field diffusion inside GO SiFe electrical steels

Elias Salloum, Olivier Maloberti, Manar Nesser, Stéphane Panier, Julien Dupuy

Identification and analysis of static and dynamic magnetization behavior sensitive to surface laser treatments within the electromagnetic field diffusion inside GO SiFe electrical steels

Elias Salloum[a], Olivier Maloberti[b], Manar Nesser[a], Stéphane Panier[a], Julien Dupuy[c]

[a]*Laboratoire des Technologies Innovantes, LTI-EA 3899, Université de Picardie Jules Verne, Amiens 80025, France*
[b]*ESIEE Amiens, 14 quai de la Somme BP10100, Amiens 80082, France*
[c]*Multitel a.s.b.l, Parc Initialis, Mons, BE 7000*

Abstract

Surface laser treatment of soft magnetic materials, such as GO SiFe electrical steels, is mainly used to reduce iron losses by modifying the static and the dynamic magnetic properties. Laser treatment effect on mesoscopic electromagnetic properties of soft magnetic materials is presented. An experimental procedure using the Single Sheet Tester is performed on a magnetized sheet with specific exciting induction level and frequency. Transient average magnetic flux density through the sample cross-section and its corresponding applied magnetic field are measured. Data are identified in the time-domain with numerical results obtained by solving the diffusion equation using a 1-D discretization approach. The identification strategy requires a material law that includes both non-linear static and dynamic properties and describes the magnetic behavior due to domains and walls dynamics. Next, parametric and physical studies are performed on materials submitted to different laser treatments in order to determine and interpret their effects on the identified magnetic properties and the time response in the sheet's depth. The results show that the static and the dynamic properties can be simultaneously improved. This analysis help to understand the impact of laser treatments on the static and the dynamic behaviour in order to improve the material magnetic performances within magnetic circuits inside electrical machines and transformers.

Keywords: GO SiFe electrical steels, Single Sheet Tester (SST), Properties identification, Static and dynamic behavior, Transient response, Finite element method (FEM), Laser treatment.

1. Introduction

Soft magnetic materials are increasingly used in electrical machines. The improvement of the magnetic performances by increasing the permeability and decreasing the iron losses is a challenge in industrial applications. One of the adopted strategies considers the use of laser surface texturizing in order to improve the magnetic performances within magnetic circuits inside electrical machines. Many studies have been performed on different laser techniques to reduce the magnetic losses. In fact, mechanical stresses are generated inside the material due to the surface laser effect, modifying the domain structure behavior [1]. Several modes (such as pulse, continuous lasers, dotted lines) and parameters (such as the laser power, speed, pitch) are adopted and optimized to allow domain refinement, reducing the magnetic losses and increasing the walls mobility [2, 3, 4]. Domain refinement can also contribute in noise optimization [5]. The macroscopic observations and results induced by laser treatment are derived from the microscopic behavior at the domain scale, concerning the energy minimization phenomenon that explains the magnetic and elastic behavior dependence to the domains rotation, walls movement and internal stresses [6, 7]. Many researches have investigated the effect of the applied mechanical stresses on the magnetic and the magneto-elastic behavior [8, 9, 10, 11, 12]; an impact on the permeability and the magnetostriction coefficient is observed. In this paper, we present the laser scribing effect on the static and dynamic magnetic behavior inside GO FeSi electrical steels. The material's magnetic properties are identified with transient measurements using the

⋆This work was carried out within the frame of the project ESSIAL, funding from the European Union's Horizon 2020, research and innovation program under grant agreement No 766437.

*Corresponding author
Email address: salloum.elias@u-picardie.fr (Elias Salloum)
URL: www.u-picardie.fr (Elias Salloum)

time dependent Maxwell's equations. The identification technique is based on an experimentation performed in the Single Sheet Tester and on the numerical results derived from the 1-D diffusion equation using the finite element discretization in the time-domain. We consider a behavioral law that includes both a static property and a dynamic damping property that homogenizes the microscopic processes related to domains and walls. The static behavior is identified using the Jiles-Atherton model [13, 14, 15, 16, 17, 18]. As for the dynamic behavior, we identify a homogenized damping magnetization property Λ [19, 20, 21] using a formulation similar to the diffusion problem presented by Raulet et al. [22]. A sensitivity analysis of the identified properties induced by laser treatment is then performed. Meanwhile, time-domain study in the sheet's cross section, including the magnetic properties and the diffusion equation is performed with a parametric analysis. This modeling strategy is one key to improve the magnetic performances in electrical machines and transformers.

2. Electromagnetic modeling

2.1. Problem

A 150x150 mm^2 GO FeSi electrical steel sheet is considered with the following properties: iron thickness $h = 0.23$ mm, magnetic anisotropy in the lamination direction of $\Delta\theta \pm 7°$, grain size between 3 mm and 8 mm, density $\rho = 7,380$ kg.m^{-3} and electrical conductivity $\sigma = 2.10^6$ $(\Omega.\text{m})^{-1}$. The experiments are performed in the Single Sheet Tester, an apparatus dedicated to the measurement of the magnetic losses and the hysteresis. The sheet is magnetized inside the bench due to the presence of a uniform, in-plane and cycling magnetic field in the surrounding of the sheet (Fig. 1). This field is induced by the electrical currents generated in the primary coils. The problem consists in measuring the surface magnetic field $H_a(t)$ needed to magnetize the sheet with a specific average induction $B_{av}(t)$ characterized by a magnitude (induction level), a frequency and a signal shape. The latter is determined by the secondary coils of the bench. The collected data provide only macroscopic observations related to the magnetic behavioor; a measurement identification with a specific diffusion model is then performed for this purpose, deriving at the meanwhile the static and the dynamic properties that fit the model with the measurements.

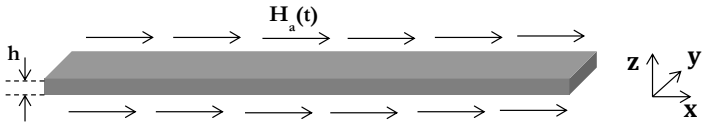

Fig. 1. Magnetization process in the SST

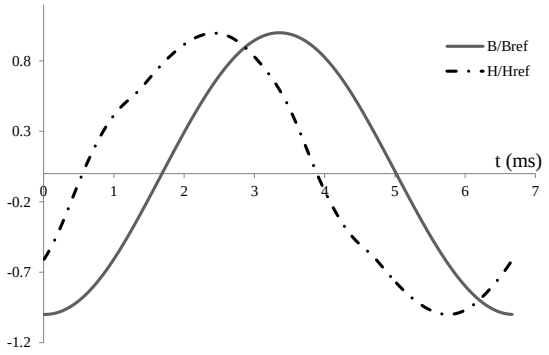

Fig. 2. Transient signals collected from the SST measurement.

2.2. Magnetic modeling: the Diffusion Equation

The electromagnetic behavior at the local space of the sample is modeled using the Maxwell's equations (Eqs. 1) that include both space and time dependence. This technique is more like a phenomenological modeling in

the case of grain-oriented materials, where the cross section contains one grain. Therefore, the presented model represents a statistical approach for the global behavior of the sheet.

$$\mathbf{rot}(\mathbf{H}) = \mathbf{J} \qquad \mathbf{rot}(\mathbf{E}) = -\frac{\partial \mathbf{B}}{\partial t} \tag{1}$$

J, **E**, **B** and **H** are the local vectors that correspond to the current density, the electrical field, the magnetic flux density and the magnetic field respectively. The problem presented in 2.1 reduces the complexity of the model to a 1-D analysis thanks to different contributions:

1. The geometry is symmetric with respect to the xy plane in the SST.
2. The in-plane dimensions are more significant than the thickness.
3. The applied magnetic field in the x direction is symmetric with respect to the z-axis and uniform on the surface.
4. Measurements are only collected in the x direction.

When the surface magnetic field is applied in the x direction, the magnetization occurs in all directions due to the anisotropy. However, we only consider the magnetization in the lamination direction (x direction) because measurements are only given in the longitudinal direction. The horizontal variables vary with the sheet's cross-section(z direction). Considering a linear electrical behavior ($\mathbf{J} = \sigma\mathbf{E}$), the 3-D Maxwell's equations are reduced to a 1-D diffusion equation (Eq. 2), including the eddy current losses generated by the electromagnetic energy exchange. A 1-D differential equation with two local variables is obtained:

$$\frac{\partial^2 H(z,t)}{\partial z^2} = \sigma \frac{\partial B(z,t)}{\partial t} \qquad H(\pm\frac{h}{2}, t) = H_a(t) \tag{2}$$

2.3. Dynamic behavioral law

The solution requires the consideration of the magnetic behavioral law that locally correlates both variables $H(z,t)$ and $B(z,t)$. The dynamic behavior was presented by Bertotti explaining the presence of excessive losses next to the static and eddy current losses in the magnetized medium. In fact, the dynamics of walls in the microscopic scale generate a delay between the local flux density and the magnetic field; the material locally subjected to a magnetic field is magnetized with a delay related to the walls mobility, surface and density. Maloberti et al. [19] presented an homogenization of this behavior using a macroscopic damping property Λ, homogeneous to a length, and including different microscopic physical characteristics:

$$\Lambda = \sqrt{\frac{1}{2\sigma\zeta J_s n_w m_w S_w}} \tag{3}$$

σ is the electrical conductivity, $0 < \zeta < 1$, J_s the saturation magnetic polarization, n_w the average walls density, m_w their average mobility, S_w their mean surface.
The dynamic law considered by Maloberti et al. [20] considers a static behavior $H_s(B)$ modeled by the material's permeability and a dynamic damping behavior H_{dyn} characterized by the damping property Λ.

$$\begin{aligned} H(z,t) &= H_s(z,t) + H_{dyn}(z,t) \\ H(z,t) &= H_{s_B}(z,t) + \sigma\Lambda^2_{(B,\frac{\partial B}{\partial t})}\frac{\partial B(z,t)}{\partial t} \end{aligned} \tag{4}$$

The static contribution is independent of the exciting frequency; it follows a static non-linear law that can be identified by the Jiles-Atherton model and measured at very low frequencies (3 Hz). Meanwhile, the dynamic contribution represents the damping component that involves a delayed induction with respect to the applied magnetic field. It is characterized at any frequency and any induction magnitude using the Maxwell diffusion equation. We note that the considered behavioral law includes the non-linearities observed in the grain-oriented material due to the large size of the grains in such materials. Therefore, the identification technique is performed separately for each induction magnitude and frequency couple.

3. Analytical analysis of the diffusion problem

The effect of the static and the damping magnetic properties on the diffusion and the dispersion in the cross section is presented using an analytical solving of the diffusion equation.

3.1. Analytical solution

We present the analytical linear solution of the diffusion equation (Eq. 2) corresponding to a sinusoidal input/output system corresponding to the problem described in section 2.1. Assuming that the different properties (static permeability μ without losses and dynamic damping property Λ) of Eq. 4 are constant, the diffusion differential equation is analytically solved. A dispersion equation is obtained using the Fourier time and space transform [20].

$$k^2(1 + j\sigma\Lambda^2\mu\omega) + j\sigma\mu\omega = 0 \tag{5}$$

where $k = k = k_- - jk_+$ and $k_\pm(\mu, \Lambda, \sigma, \omega) = \sqrt{\frac{1}{2}\left(\frac{\mu\sigma\omega}{1+(\sigma\Lambda^2\mu\omega)^2}\right)\left(\pm\sigma\Lambda^2\mu\omega + \sqrt{1+(\sigma\Lambda^2\mu\omega)^2}\right)}$ The problem considers the determination of the applied magnetic field for a given average induction.

$$\tilde{H}_a = \frac{h(k_+ + jk_-)(1 + j\sigma\Lambda^2\mu\omega)}{2\mu\tanh((k_+ + jk_-)h/2)}\tilde{B}_{av} \tag{6}$$

The determination of the surface magnetic field (Eq. 6) allows the calculation of the local flux density's complex magnitude and derives a time response of this variable:

$$B(z,t) = |\tilde{B}(z)|\cos(\omega t + \varphi) \tag{7}$$

The proposed analytical solution calculates the local dynamic behavior based on the knowledge of the magnetic properties and a given average magnetic field. It is also the key to determine the effect of the magnetic properties on the dynamic local response (section 3.2).

3.2. Sensitivity of the dynamic response to the static and dynamic properties

The transient response of the flux density is calculated for different static μ and dynamic Λ properties using the linear analytical approach developed in section 3. This parametric study helps to understand the effect of magnetic properties and eventually the effect of the laser treatment sensitive to the magnetic properties. The reference parameters are: the thickness $h = 0.23\ mm$, the average induction magnitude $|\tilde{B}_{av}| = 1\ T$, the induction angle 0 rad, the exciting frequency $f = \omega/2\pi = 1000Hz$ and the electrical conductivity $\sigma = 2.10^6(\Omega.m)^{-1}$. The variable parameters are the relative permeability $\mu_r = \mu/\mu_0$ and the dynamic property Λ. The effect of the static property μ_r and the dymanic property Λ in terms of magnitude and delay is observed by comparing the local induction with the average induction with respect to the magnetic field on one hand (Figs. 3 and 4), and with respect to the average induction on the other hand (Figs. 5 and 6). The increase of the permeability induces an increase in the dispersion of the flux density profile (skin effect) as shown in Fig. 3. The magnitude and the delay of the induction with respect to the magnetic field increase. On the other hand, the decrease of the dynamic property (domains refinement) leads to an increase in the profile's dispersion with respect to the magnetic field as shown in Fig. 4. The magnitude increases and the induction's delay with respect to the magnetic field decreases when decreasing Λ. Figs. 5 and 6 plot the distribution of the magnitude and the angle of the flux density in the cross section for different values of μ_r and Λ and with respect to the average induction. The increase of the permeability induces an increase in the dispersion of the flux density magnitude profile (Fig. 5a) and an increase in the dispersion of the flux density phase profile for a limit of $\mu_r = 5000$ then a decrease of the profile dispersion (Fig. 5b). On the other hand, the decrease of the dynamic property leads to an increase in the magnitude dispersion with an optimum at Λ=100μm followed by a decrease (Fig. 6a). As for the angle between the local and the average induction, its profile is more dispersed when Λ decreases (Fig. 6b).

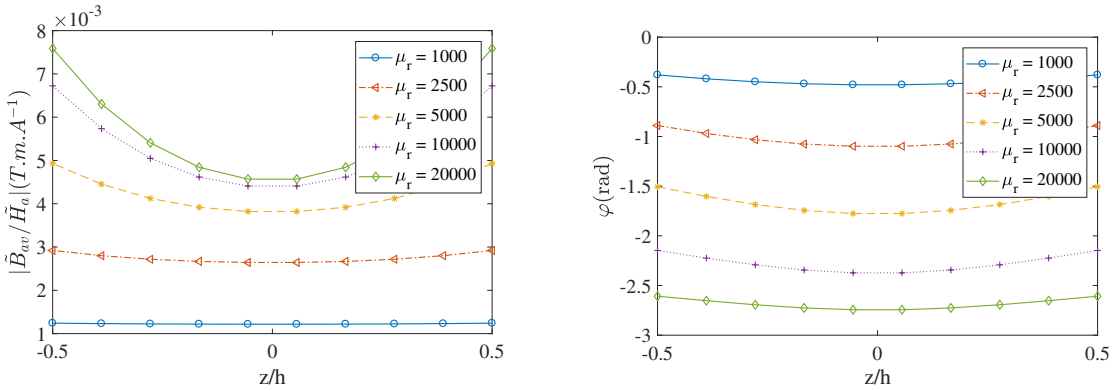

(a) Magnitude distribution **(b)** Delay distribution

Fig. 3. Effect of μ_r on the flux density distribution with respect to the applied magnetic field.

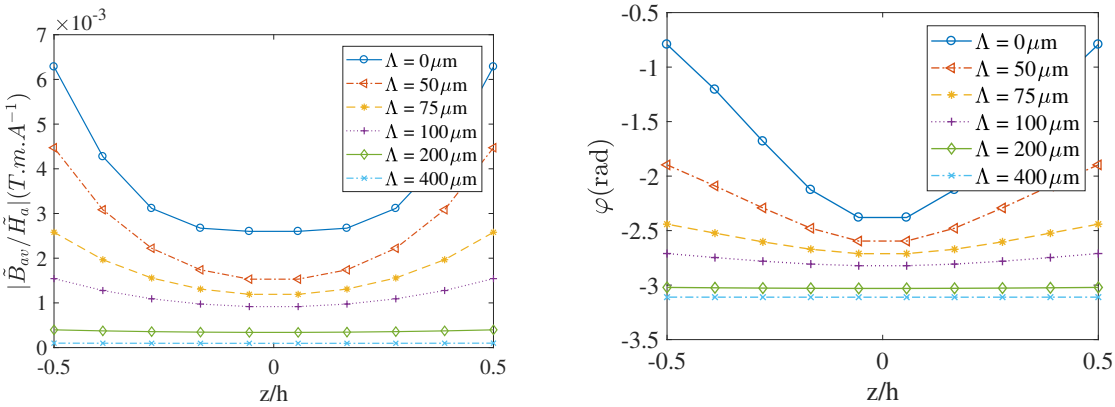

(a) Magnitude distribution **(b)** Delay distribution

Fig. 4. Effect of Λ on the flux density distribution with respect the applied magnetic field.

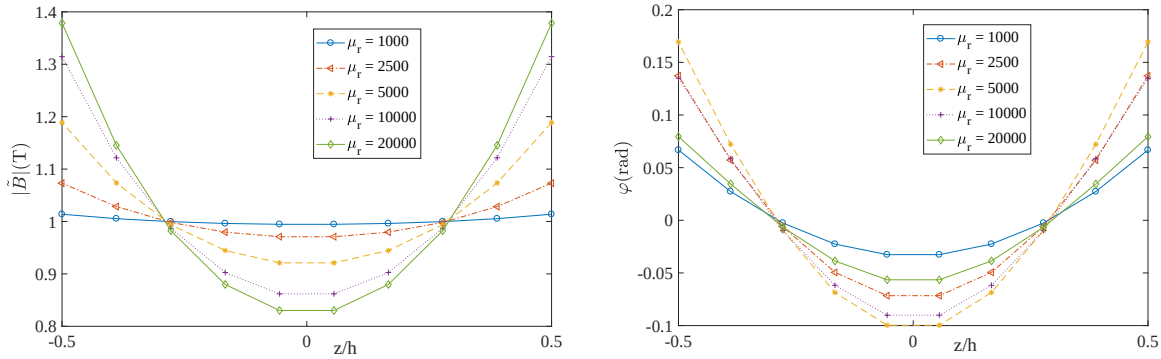

(a) Magnitude distribution (around 1 T) **(b)** Delay distribution (around 0 rad)

Fig. 5. Effect of μ_r on the flux density distribution in the cross section.

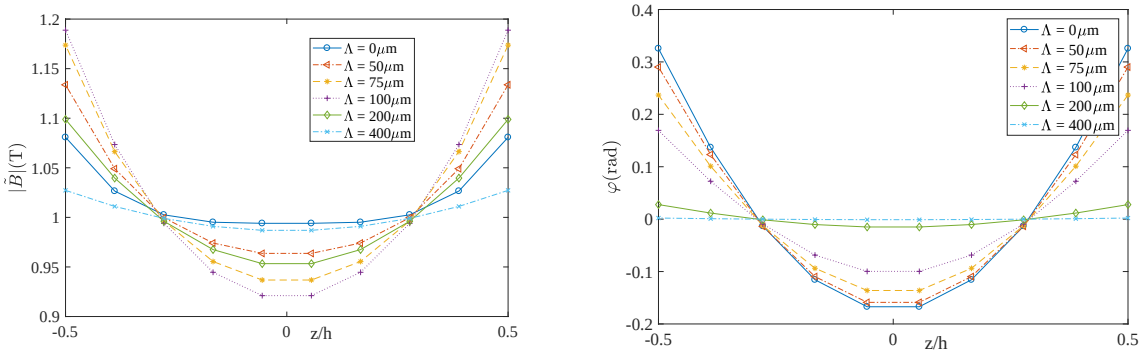

(a) Magnitude distribution (around 1 T) **(b)** Delay distribution (around 0 rad)

Fig. 6. Effect of Λ on the flux density distribution in the cross section.

4. Magnetic properties identification

The measured signals $H_a(t)$ and $B_{av}(t)$ in the SST are identified with a numerical model that allows the determination of the magnetic behavioral law and enables the knowledge of the local variables that vary with the sheet's cross section. In this case, the analytical solution proposed in section 3 cannot be used due to the non-linearity of the magnetic properties. Therefore, a numerical discretization approach is adopted.

4.1. Static Behavior: The Jiles-Atherton Model

The static behavior at a specific induction magnitude is identified using the Jiles-Atherton model. In fact, the static behavior is observed for a very low exciting frequency (3 Hz), where the dynamic behavior is neglected. Based on the Jiles-Atherton model [13], we consider the observable signals: the applied magnetic field $H_a(t)$ and the average magnetisation by $M_{av}(t) = B_{av}/\mu_0$. We consider the Jiles-Atherton model:

$$H_{eff} = H_a + \alpha M_{av} \tag{8}$$

$$M_{an} = M_s \left[\coth\left(\frac{H_{eff}}{a}\right) - \frac{a}{H_{eff}} \right] \tag{9}$$

$$\frac{dM_{irr}}{dH_{eff}} = \frac{M_{an} - M_{irr}}{k\delta} \tag{10}$$

$$M = (1-c)M_{irr} + cM_{an} \tag{11}$$

$$\delta = \begin{cases} 1, & \text{if } \frac{dH_a}{dt} > 0 \\ -1, & \text{if } \frac{dH_a}{dt} < 0 \end{cases} \tag{12}$$

H_{eff}, M_{an}, M_{irr} are respectively the effective magnetic field, the anhysteretic magnetization and irreversibility magnetization. α, a, M_s, k and c are the Jiles-Atherton parameters to be identified. We notice that the static hysteresis is not replicable for all the induction magnitudes when using this model. Therefore, the model is identified for each induction magnitude seperately and different values of the model's parameters are collected for each induction level. The aim of this identification is to compare the static behavior for laser configurations (before and after treatment) and to identify later on the behavior at higher frequencies.

The hysteresis loops are rebuilt using the Jiles-Atherton (JA) model and compared with the measurements as shown in Fig. 9. A high accuracy is observed when identifying each induction magnitude alone and we notice that it decreases for high induction magnitudes (1.5 T).

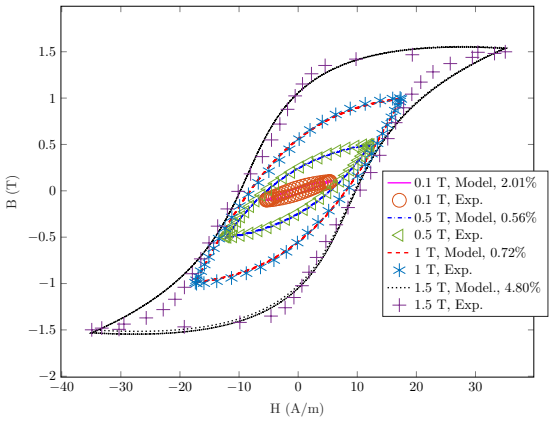

Fig. 7. Comparison between the static measurement and the Jiles-Atherton fitting model for a reference sample.

4.2. Identification of the damping property

The dynamic problem (Eq. 2) includes a z-direction dependence. This constraint is solved with the finite element method using 1-D quadratic shape functions with a 3-nodes element. The quadratic methodology gives accurate results for a limited number of elements. Combining the diffusion equation with the boundary condition in Eq. 2 and considering a time discretization Δt equal to the measurement's sampling period one gets:

$$\frac{\sigma}{\Delta t}(\Lambda^2\mathbf{U}+\mathbf{V})\mathbf{B}(t)+\mathbf{U}\mathbf{H_s}(t)=\mathbf{f}(t)+\frac{\sigma}{\Delta t}(\Lambda^2\mathbf{U}+\mathbf{V})\mathbf{B}(t-1) \tag{13}$$

$\mathbf{U}$ and $\mathbf{V}$ are nodal matrices, assembled from elementary matrices dependent on the local shape functions and $\mathbf{f}(t)$ is the system's input including the applied magnetic field on the boundaries, $\mathbf{B}$ is a discretized local flux density vector and $\mathbf{H_s}$ is the static discretized local magnetic field vector dependent on $\mathbf{B}$.

The damping property Λ depends on the induction magnitude and the excitation frequency [20]. Similar to the static identification, the calculation of Λ is performed in each cycle using the discretized diffusion equation (Eq. 13) assuming a constant property through each measured cycle. The dynamic identification requires the knowledge of the static behavior ($H_s = f(B)$) presented in section 4.1. Eq. 13 calculates the local magnetic flux density vector $\mathbf{B}$ from which the average induction is directly derived ($B_{av}(t) = \int_{-\frac{h}{2}}^{\frac{h}{2}} B dz$). The identification of Λ consists in minimizing the error between the measured cycle and the numerically calculated cycle using the R-squared method. The optimization method uses a very simple technique presented by Lagarias et al. [23] and implemented in Matlab. Cycles are then rebuilt, showing the similarity between the measured and the modeled cycles as plotted in Fig. 8. The latter also shows the modeled cycle without considering the dynamic property (only eddy currents), the measured and calculated static cycles using the JA method, the mid-anhysteretic curve that is defined by the middle curve of the static loop and the anhysteretic curve identified by the JA method.

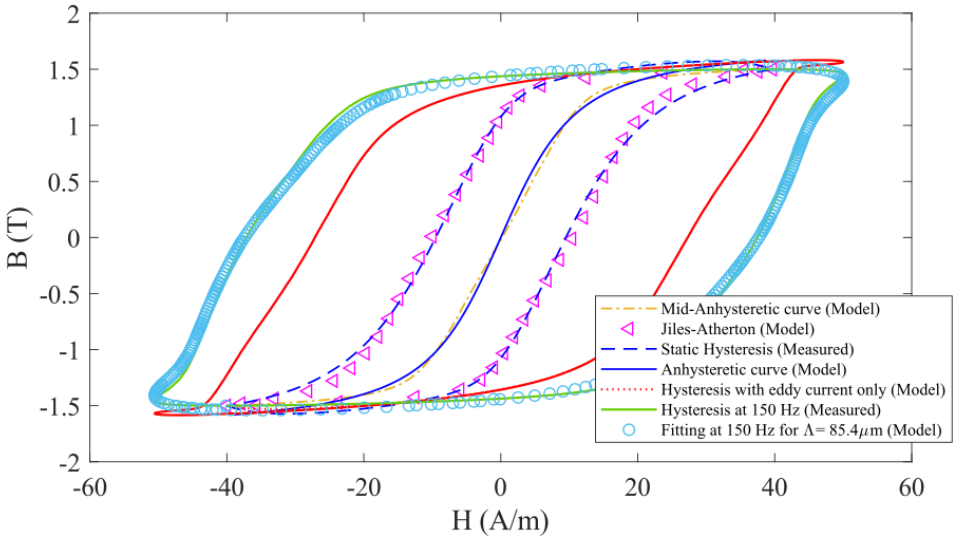

Fig. 8. Modeled and measured, static and dynamic hysteresis loops for a reference sample

5. Sensitivity analysis to surface laser treatments

5.1. Laser treatment configurations and strategies

The effect of surface laser treatments on the static and dynamic properties identified in section 4 is carried out. Different laser treatment configurations are applied on the sample's surface. We observe a dispersion between the different reference samples. Therefore, measurements are performed on the reference sample before treatment and then after treatment, in order to insure more accurate and stronger conclusions regarding the treatment's effect. Table 1 presents the different reference samples with the same geometric properties and their corresponding laser treatment and laser parameters.

Reference sample	Laser Treatment	Mode	Pulse width
Ref. 1,2	Ultra-short pulse (F500)	Ablation	500 fs
Ref. 3,4	Short pulse (N4)	Scribing	4 ns
Ref. 5,6	Long pulse (N100)	Irradiation	100 ns
Ref. 7,8	Continuous wave pulse (CW)	Irradiation	-

Table 1
Laser treatments applied on the reference samples

5.2. Effect on the static property

The sensitivity of the static behavior to the laser treatment is presented. Considering the Jiles-Atherton model presented and identified in section 4.1, the static hysteresis loops and the Langevin functions corresponding to the different laser configurations are shown in Figs. 9 and 10 at 1.5 T and 0.5 T respectively. The a parameter of the anhysteretic qualifies the material's permeability; a decrease of a means a higher permeability. Laser treated samples are analyzed in Fig. 11 in comparison with the reference samples. The anhysteretic curve becomes steeper for the ultra-short, short and long pulse lasers. However, a high amount of magnetic field is needed at high frequencies for the same induction magnitude. On the other hand, the slop decreases for the continuous wave configurations. In addition, the static irreversibility can be analyzed using Figs. 9 and 10; we observe a small reduction in the coercivity for the long pulse, short pulse and ultra-short pulse lasers.

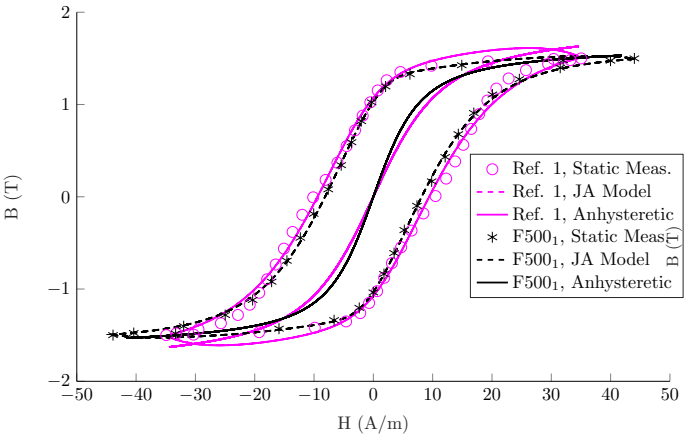

(a) Ref. 1

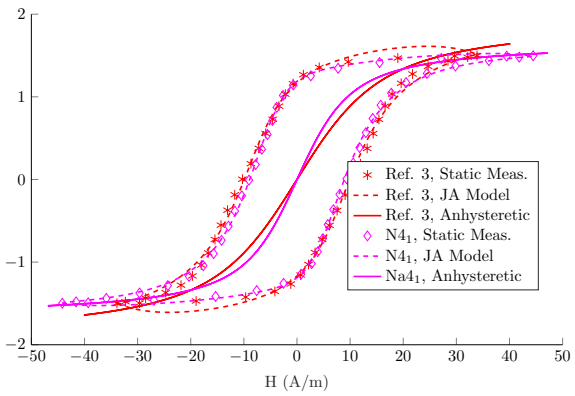

(b) Ref. 3

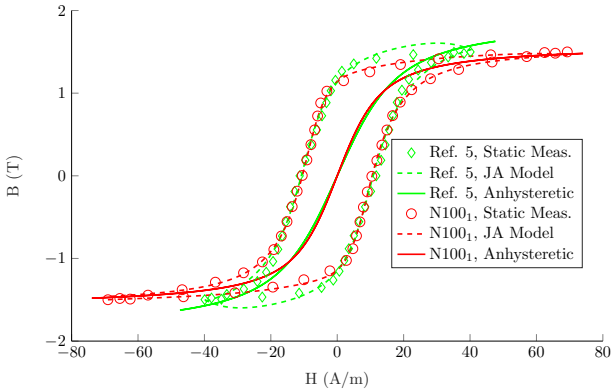

(c) Ref. 5

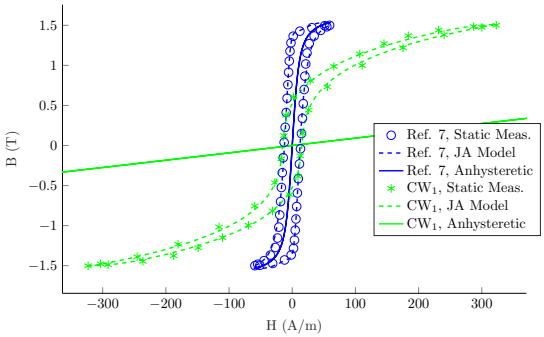

(d) Ref. 7

Fig. 9. Sensitivity of the static behavior to the laser treatments at 1.5 T

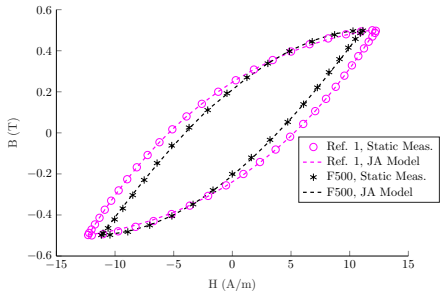

(a) Ref. 1

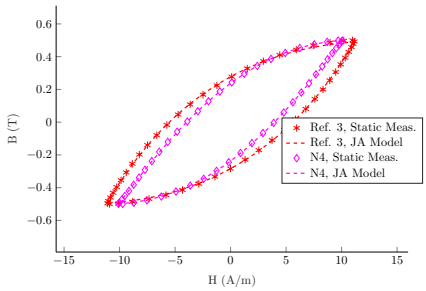

(b) Ref. 3

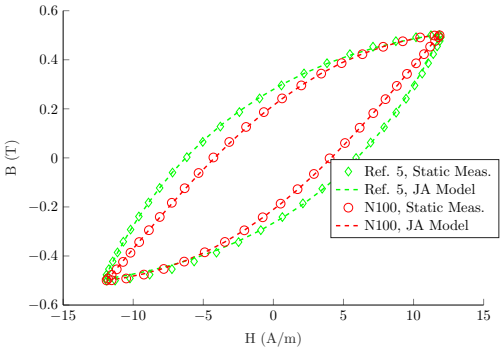

(c) Ref. 5

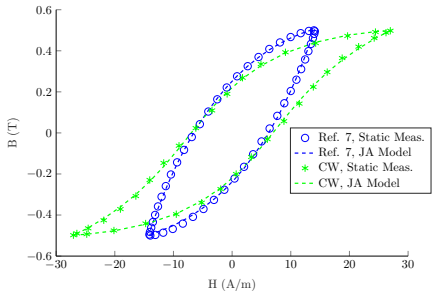

(d) Ref. 7

Fig. 10. Sensitivity of the static behavior to the laser treatments at 0.5 T

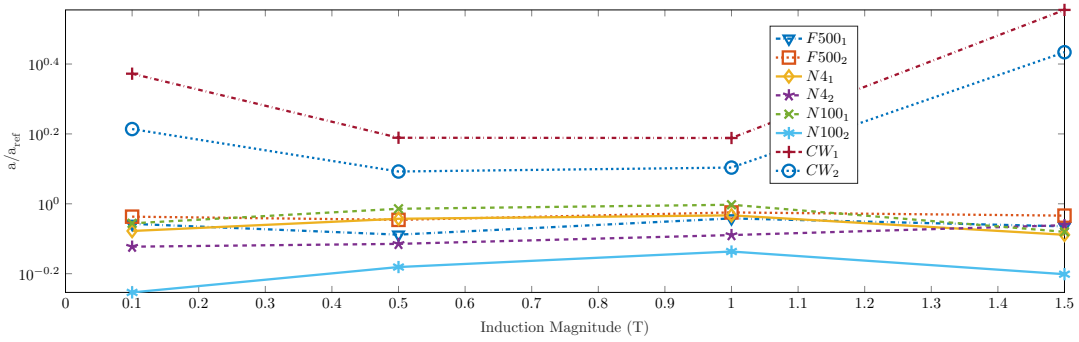

Fig. 11. Comparison of the Jiles-Atherton's parameter a of the treated samples with the reference sample's parameter a_{ref}

5.3. Effect on the damping property

The identification of the dynamic damping property Λ performed in section 4.2 at different frequencies and induction levels is applied for the different laser configurations, showing their effect on the dynamic behavior. Λ/Λ_{ref} represents the ratio between the dynamic property for a given configuration and the property of its corresponding reference sample. It is shown in Fig. 12 that the dynamic property decreases for the long pulse, short pulse and

ultra-short pulse lasers. However, the continuous wave laser increases the dynamic property in all cases. The change of this property means a variation in the dynamic structural behavior at the domain scale; a decrease of Λ means a higher walls mobility, higher walls density and/or a higher walls surface. These volume properties modification are induced from the surface laser treatment; the application of laser on the surface generates a new equilibrium state and the domain volume structure is reorganized a way to minimize the total energy. As a result, the hysteresis loop for high frequencies is modified; a smaller Λ means a reduced hysteresis area as shown in Figs. 13.

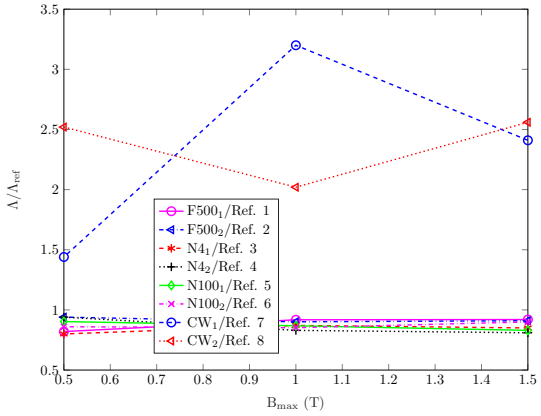

(a) Variation of Λ at 50 Hz

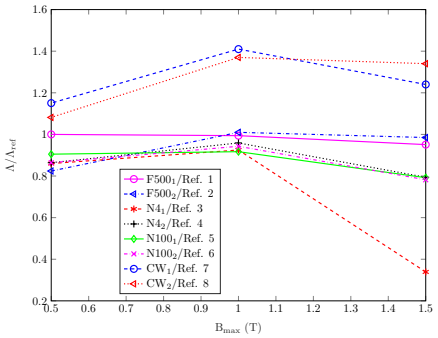

(b) Variation of Λ at 150 Hz

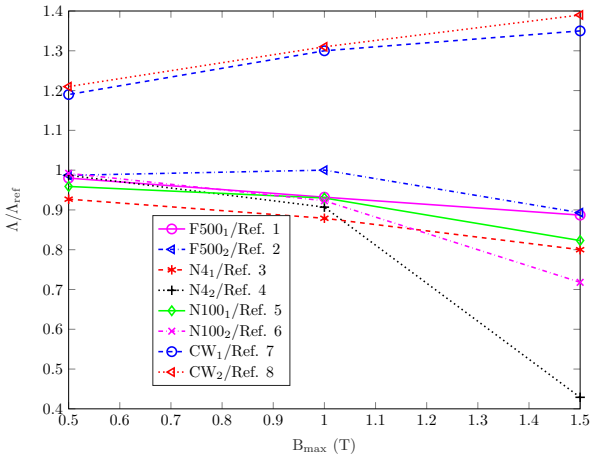

(c) Variation of Λ at 500 Hz

Fig. 12. Sensitivity of the damping property Λ to the laser treatment at different frequencies

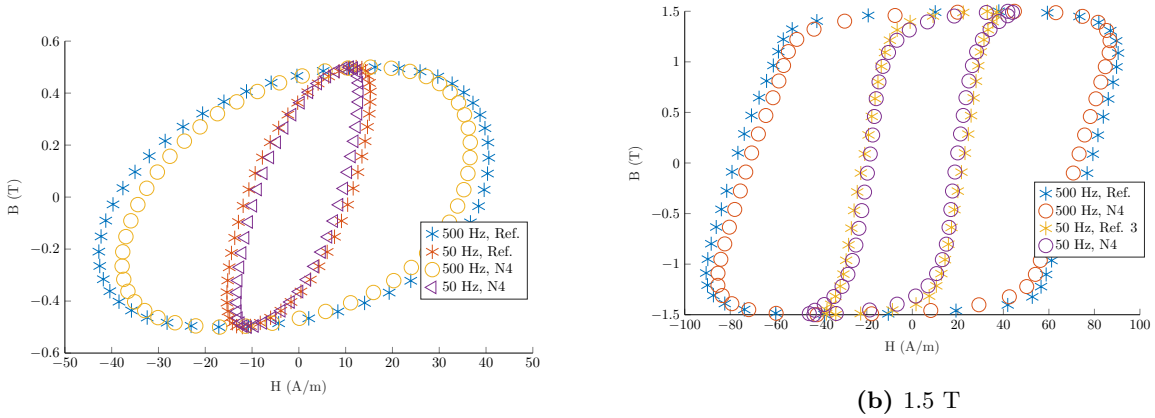

(a) 0.5 T

(b) 1.5 T

Fig. 13. Comparison of the hysteresis cycles between the reference sample and the ultra-short pulse sample

5.4. Effect on the dynamic response

As presented in section 5, the magnetic properties are sensitive to the laser treatment; they can be improved or deteriorated. Based on the identified magnetic properties (static and dynamic) sensitive to the laser configurations, the effect on the transient response of the local flux density is studied. The dispersion decreases for the long pulse, ultra-short pulse and short pulse laser in terms of amplitude and increases in term of phase. Fig. 14 illustrates the flux density's time response at the surface and in the middle of the cross section for the long pulse laser at 1.5 T induction level and 500 Hz frequency.
On the other hand, the local induction signal (at the surface and in the middle section) is not perfectly sinusoidal even if the average induction is sinusoidal. In fact, the diffusion and dispersion phenomena combined with a non-linear static property, specially at high induction, induce harmonics in the local induction signal and requires a magnetic field signal with harmonics.

6. Conclusion

Static and dynamic magnetization properties sensitive to surface laser treatments within the electromagnetic field diffusion are analyzed and identified inside GO SiFe electrical steels. The diffusion equation is adopted to model the magnetic behavior, including static and dynamic properties that define the magnetic behavior. The model is identified with measurements performed in the Single Sheet Tester from which the magnetic properties and the local behavior are derived. This identification technique allows the determination of the laser treatment's effect on static and dynamic properties on one hand, and the dynamic response on the other hand. An increase in the static property and a decrease in the dynamic property are observed for the long pulse, short and ultra-short pulse lasers in comparison with the reference samples before treatment. However, a decrease in the static property and an increase in the dynamic property are observed in the continuous wave laser. The dynamic response study in the frequency and the time domains shows a lower profile dispersion in the ultra-short, short and long pulse lasers. These results, in addition to the harmonic analysis generated from both the diffusion phenomenon and the non-linear behavior are the key for analyzing the magnetic and the mechanical behavior inside electrical machines sensitive to the magnetic behavior and eventually laser treatment.

Acknowledgement

This work was carried out within the frame of the project ESSIAL, funding from the European Union's Horizon 2020, research and innovation program under grant agreement No 766437.

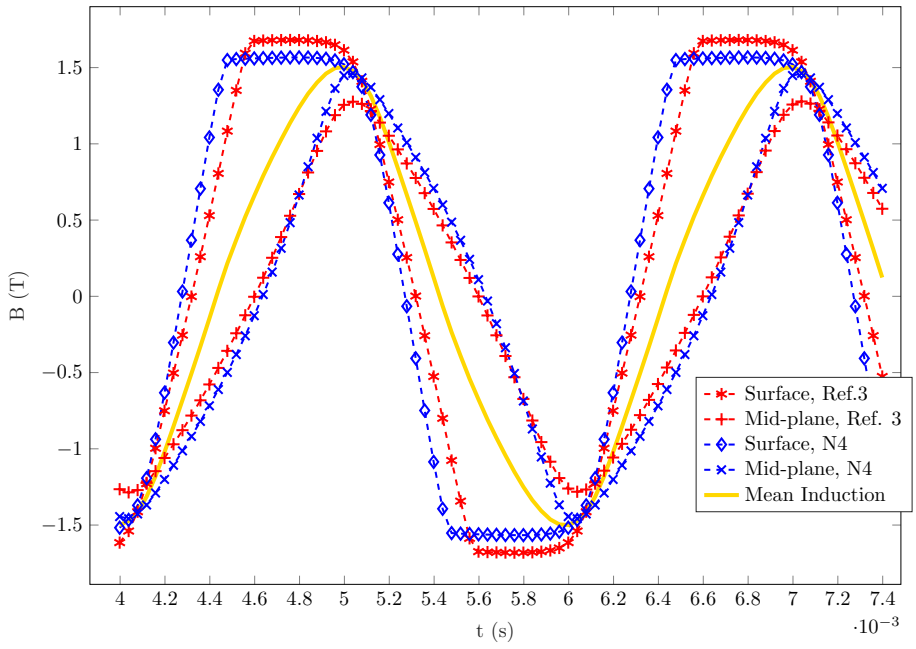

Fig. 14. Transient response of the surface and the middle section flux density for the Ref. 3 sample

References

[1] S. Patri, R. Gurusamy, P.A. Molian, and M. Govindaraju. Magnetic domain refinement of silicon-steel laminations by laser scribing. *Journal of materials science*, 31(7):1693–1702, 1996.

[2] M. J. Johnson, R. Chen, and D. C. Jiles. Reducing Core Losses in Amorphous $Fe_{80}B_{12}Si_8$ Ribbons by Laser-Induced Domain Refinement. *IEEE Transactions on Magnetics*, 35(5):3865–3867, 1999.

[3] T. Kajiwara and M. Enokizono. Effect of Laser Stress on Vector Magnetic Properties of Electrical Steel Sheets. *IEEE Transactions on Magnetics*, 50(4):2002404, 2014.

[4] A. Zeleňáková, P. Kollár, M. Kuźmiński, M. Kollárová, Z. Vértesy, and W. Riehemann. Magnetic properties and domain structure investigation of laser treated finemet. *Journal of Magnetism and Magnetic Materials*, 254:152–154, 01 2003.

[5] L. Lahn, C. Wang, A. Allwardt, T. Belgrand, and J. Blaszkowski. Impoved Transformer Noise Behavior by Optimized Laser Domain Refinement at ThyssenKrupp Electrical Steel. *IEEE Transactions on Magnetics*, 48 (4):1453–1456, 2012.

[6] G. Bertotti. Connection between microstructure and magnetic properties of soft magnetic materials. *Journal of Magnetism and Magnetic Materials*, 320(20):2436–2442, April 2008.

[7] F. Alves and R. Barrué. Magnétisme microscopique à l'échelle des domaines magnétiques dans les matériaux ferromagnétiques doux. *J3eA*, 3(6), 2004.

[8] U. Aydin, P. Rasilo, D. Singh, A. Lehikoinen, A. Belahcen, and A. Arkkio. Coupled Magneto-Mechanical Analysis of Iron Sheets Under Biaxial Stress. *IEEE Transactions on Magnetics*, 52(3), 2015.

[9] U. Aydin, P. Rasilo, F. Martin, D. Singh, L. Daniel, A. Belahcen, M. Rekik, O. Hubert, R. Kouhia, and A. Arkkio. Magneto-mechanical modeling of electical steel sheets. *Journal of Magnetism and Magnetic Materials*, 439:82–90, 2017.

[10] Katarzyna Fonteyn, Anouar Belahcen, Reijo Kouhi, Paavo Rasilo, and Antero Arkkio. FEM for Directly Coupled Magneto-Mechanical Phenomena in Electrical Machines. *IEEE Transactions on magnetics*, 46(8): 2923–2926, 2010.

[11] K. A. Fonteyn. *Energy-based magneto-mechanical model for electrical steel sheets*. PhD thesis, Aalto University, School of Electronics, Communications and Automation, 2010.

[12] A. Belahcen. *Magnetoelasticity, magnetic forces and magnetostriction in electrical machines*. PhD thesis, University of technology Helsinki, 2004.

[13] D. C. Jiles and D. L. Atherton. Theory of ferromagnetic hysteresis. *Journal of Magnetism and Magnetic Materials*, 61(1):48–60, 1986.

[14] R. Szewczyk and Jacek Salach A. Bienkowski. Extended jiles-atherton model for modelling the magnetic characteristics of isotropic materials. *Journal of Magnetism and Magnetic Materials*, 320(20):e1049–e1052, April 2008.

[15] F. B. R. Mendes, J. V. Leite, N. J. Batistela, and N. Sadowski. An improved method for acquisition of the parameters of jiles-atherton hysteresis scalar model using integral calculus. *Journal of Microwaves, Optoelectronics and Electromagnetic Applications*, 16(1):165–179, March 2017.

[16] D. C. Jiles, J. B. Thoelke, and M. K. Devine. Numerical determination of hysteresis parameters for the modeling of magnetic properties using the theory of ferromagnetic hysteresis. *IEEE Transactions on Magnetics*, 28(1): 27–35, January 1992.

[17] K. Chwastek, J. Szczyglowski, and M. Najgebauer. A direct search algorithm for estimation of jiles-atherton hysteresis model parameters. *Materials Science and Engineering: B*, 131(1):22–26, 2006.

[18] Nicusor Pop and Ovidiu Caltun. Jiles-atherton model in fitting hysteresis curves of magnetic materials. *Journal of Optoelectronics and Advanced Materials*, 13:537–543, 05 2011.

[19] O. Maloberti, A. Kedous Lebouc, G. Meunier, and V. Mazauric. Field diffusion-like representation and experimental identification of a dynamic magnetization property. *Journal of Magnetism and Magnetic Materials*, 304:507–509, 2006.

[20] O. Maloberti, G. Meunier, and A. Kedous Lebouc. On hysteresis of soft materials inside formulations: Delayed diffusion equations, fields coupling, and nonlinear properties. *IEEE Transactions on Magnetics*, 44(6):914–917, 2008.

[21] O. Maloberti, V. Mazauric, G. Meunier, A. Kedous-Lebouc, P. Wendling, and B. Colin. A magnetic vector potential formulation to deal with dynamic induced losses within 2-d models. *IEEE Transactions on Magnetics*, 43(4):1205–1208, 2007.

[22] M. A. Raulet, B. Ducharne, J. P. Masson, and G. Bayada. The Magnetic Field Diffusion Equation Including Dynamic Hysteresis: A Linear Formulation of the Problem. *IEEE Transactions on Magnetics*, 40(2):872–875, 2004.

[23] J. C. Laragias, J. A. Reeds, M. H. Wright, and P. E. Wright. Theory of ferromagnetic hysteresisconvergence properties of the nelder-mead simplex method in low dimensions. *SIAM Journal of Optimization*, 9(1):112–147, 1998.